26

Sintering of Transparent Conductive Oxides: From Oxide Ceramic Powders to Advanced Optoelectronic Materials

Guido Falk
Saarland University, Chair Powder Technology of Glass and Ceramics, Saarbruecken, Germany

1. Introduction

Since Cadmium thin films have been sputtered and thermally oxidized for the first time in 1907 (Chopra, et al., 1983) the technological innovation in transparent conductive oxides (TCO) has developed rapidly and substantially during the last years. Indium-tin-oxide (In:90:Sn:10, ITO) is today the most important TCO material due to the potential combinations of high electrical conductivity in the range of 10^4 S/cm and high transparency in the visible range of 90 % with a layer thickness of 100 nm.

Today TCO thin films are processed by chemical or physical vapour deposition, especially vacuum based sputtering and evaporation processes. Due to these elaborate and complex manufacturing, especially for large-size TCO applications direct structuring of TCO layers by printing, sol-gel coating and other powder- and paste-based manufacturing processes have been the subject of many investigations (Hyatt, 1989, Straue, et al., 2009).

These as-processed TCO materials serve as transparent electrodes in liquid crystal displays, thin-film electroluminescence displays, electrochromic displays, transparent conductive coatings of highly sensitive radiation detectors, ferroelectric photoconductors and memory devices, transparent conductive oxidic films as gate-electrodes for injection and charge coupled devices and are used in products as flat panel displays, touchscreens, organic light emitting diodes, electroluminescence lamps as well as numerous components of solar technology.

Resulting from the increased indium consumption and the expected supply gap of indium raw materials within the next decades (Carlin, 2007) an increasing priority is attributed to the development of suitable substitute materials, whereas currently aluminium doped zinc oxide (ZnO:Al, AZO) have consistently attached the highest importance (Ellmer, et al., 2008). Beside the TCO applications mentioned above AZO is used in highly promising developments such as blue and ultraviolet lasers, components of improved light amplification of GaN-based LEDs, transparent thin film transistors, photo detectors, varistors, catalysts and optical current transformers.

Sputtered Al:ZnO thin films have already been used in commercially available flat panel displays und thin layer solar cells with an electrical resistance of 1-3 $\cdot 10^{-4}$ Ω cm at aluminium doping concentrations between 1.6 to 3.2 at.-% (Anders, et al., 2010).

Among others current research is focussing on sputtering process stability based on ITO target materials, on AZO target materials with improved electrical conductivity, thermal and mechanical stability as well as highest transparency of TCO thin layers by enhanced optimization of chemical composition, microstructure tailoring and advanced sintering and densification methodologies of TCO target materials.

2. Microstructure-property relationship of TCO materials

2.1 Nodule formation

Nodules, also called „black growths" or „black crystals", are conical defects formed during the sputtering process on the surface of the target material. The influence of nucleation on nucleus growth of nodules was investigated by camera monitoring (Schlott, et al., 1996). It was found, that especially impurities originating from the sputtering process, i.e. SiO_2 or Al_2O_3 particles , were collected on the target material and act as nucleus in the nodule formation process.

There are also other important impurities in the form of inclusions that originates from the target manufacturing process. Target materials that happen to feature the increased densification, are more suitable for sputtering processes since they exhibit fewer nodule failures (Schlott, et al., 1995, Gehman, et al., 1992). The shape of nodules has been investigated by SEM analysis and partly a distinct peak is observed, partly a flattened conical shape is formed (Schlott, et al., 1996). From time to time spherical globule like particles are observed at the nodules peak being identified as SiO_2 and Al_2O_3. In this case the particles could be assigned to impurities of the sputtering process being directly related to the nodule formation process. It was found by further detailed investigations that the external layer of the nodules contains pure ITO phase, the thickness of the layers being up to several tens of microns. Additionally these layers containing fewer oxygen concentrations compared to the bulk target material are supposed to be formed by self-sputtering. Self-sputtering means that the target itself was coated by the sputtering process as it is shown schematically in Figure 1. The oxygen deficiency can be explained by the fact that the atmosphere nearby the target surface contains less oxygen.

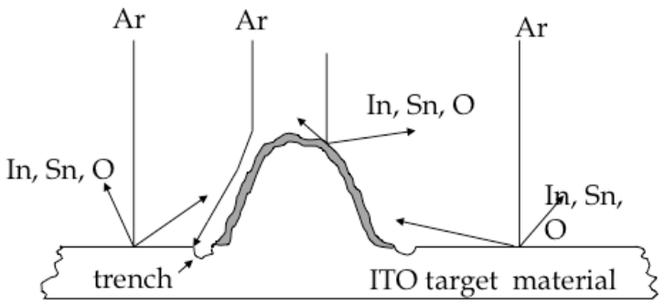

Fig. 1. Cross section scheme of a nodule formed on the surface of an ITO sputtering target according to (Schlott, et al., 1996).

Nodules have to be avoided, since they modify the sputtering process and it is therefore necessary to interrupt the process and to clean or even to exchange the target material. Nodule formation is a severe problem since nodules show a reduced sputtering voltage compared to the surrounding material. Thereby the nodules prevent the sputtering of the material being covered by the nodule layers. Furthermore when the nodule formation is avoided, arc discharge is not needed and the sputtering process is excecuted at increased sputtering voltages enabling to operate the facility at higher efficiencies (Nadaud, et al., 1995). The nodule formation was observed for metallic indium-tin targets during the reactive sputtering process (Schlott, et al., 1996) and also for sputtering of oxide ceramic ITO targets (Schlott, et al., 1995). The elimination of inclusions and metallic phases is predominant for the effective avaoidance of nodule formation (see Figure 2).

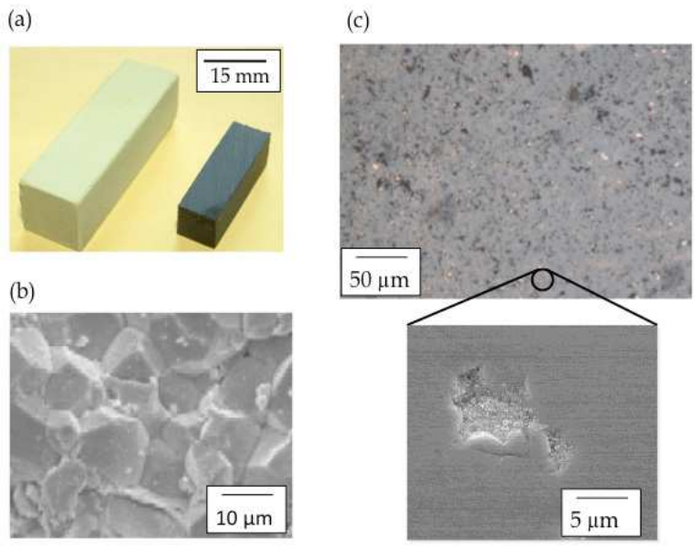

Fig. 2. Cold isostatically pressed ITO body (a, left) and sintered ITO body with a shrinkage of 15 % (a, right), SEM topography of fractured ITO surface after sintering with a mean grain size of 25 µm (b) and outbreak (dark) and segregations (bright) analysed by SEM at polished ITO surfaces (c).

A trouble-free microstructure is important to prevent the chipping (Schlott, et al., 1996). Impurties and metallic InSn eutectica have to be avoided in order to guarantee sufficient thin film qualities (Schlott, et al., 1996).

Once being formed the nodules grow contineously during the sputtering process. They do not dissolve unless they explode due to thermal stresses or due to the power of micro arc discharge effects (Schlott, et al., 1996). If that is done the desintegrated nodule particles are scattered and form nucleus of new nodules or they form small holes, so called pinholes, in the growing layer contributing to a significant quality degradation of the sputtered thin film (Kukla, et al., 1998).

Nodule formation is observed particularly frequently when the target material consists of several tiles being composed to enlarge the target surface. The split between the tiles are considered as collecting sites for impurites and dust. Furthermore the split could be coated

by self-sputtering. If an Ar atom is smashed onto these coated splits, the scattered particles composed of In, Sn and O are able to be deposited onto the sputtered thin films (Schlott, et al., 1996). A key component for the suppression of undesired nodule formation is the basic understanding of most important ITO characteristics as well as specific sintering techniques and its effectiveness to tailor distinct microstructural properties of TCO target materials. In the following sections an overview of the state of the art and future trends of the related topics are given.

2.2 The system ITO and related defect structures

Enoki (Enoki, et al., 1991) proposed the following In_2O_3-SnO_2 phase diagram shown in Figure 3.

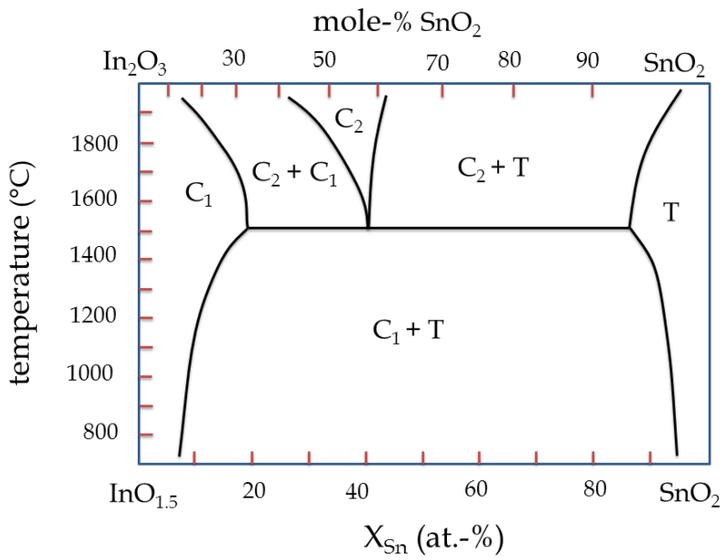

Fig. 3. Phase diagram of the pseudo-binary system In_2O_3-SnO_2 (χ_{Sn} = atom concen-tration of tin (%)).

Hereby the abbriviations C_1 and C_2 represent the cubic ITO phase and the orthorhombic intermediate respectively, and T is the rutile type SnO_2. It was found that the C_2 phase is formed in the concentration range between 47.9 and 59.3 mole-% Sn at temperatures exceeding 1573 K.

Morover it was oberserved that the intermediate (C_2) falls apart into In_2O_3 (C_1) and the T-phase according to the following eutectic reaction:

$$C_2 \leftrightarrow C_1 + T \tag{1}$$

Finally it was observed that the solubility limit of SnO_2 in In_2O_3 phase is between about 12.4 to 15.0 mole-% which is independent of the temperature (Enoki, et al., 1991). For some basic understanding it is helpful to consider the crystal structure of solid In_2O_3. The C type rare earth sesquioxide-or bixbyite crystal structure of Indium oxide is a variation of the cubically body-centred crystal structure (Marezio, 1966).

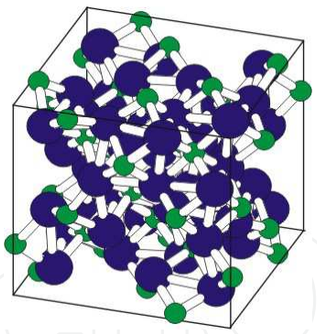

Fig. 4. Cubic In_2O_3 unit cell.

The unit cell has 80 atoms or 16 molecular weights (Warschkow, et al., 2003) and has two unequal cation positions (Granqvist & Hultaker, 2002). The lattice constant is 10.117 ± 0.001 Å (Marezio, 1966). The space group is referred to as Ia^3 or Th^7. Pure In_2O_3 has a density of 7.17 g/cm^3 (Bates, et al., 1986) and the theoretical density of the cubic structure is 7.12 g/cm^3 (Marezio, 1966). The electron subshell configuration of both atoms indium and oxygen is as follows according to (Chopra, et al., 1983):

$$O: \ 1s^2 \mid 2s^2\ 2p^4 - - \mid \tag{2}$$

$$In: \ 1s^2 \mid 2s^2\ 2p^6 \mid 3s^2\ 3p^6\ 3d^{10} \mid 4s^2\ 4p^6\ 4d^{10} \mid 5s^2\ 5p \tag{3}$$

The oxygen atoms need two more p-electrons to reach a stable 8-electron configuration. The indium atoms have three electrons in addition to a stable electron configuration. As a result the stoichiometry of the oxide is In_2O_3 resulting in a transition of electrons from In to O and a crystal structure with In^{3+} and O^{2-} ions in the lattice (Mayr, 1998). The unit cell has two unequal In-positions, the first space-diagonally (d position) and the other surface-diagonally (b position). With the d positions the oxygen atoms are located in the corners of an slightly distorted cube with two space-diagonal empty sites. In the second cube the oxygen atoms are located in a slightly differently distorted cube with two surface-diagonal empty sites. The characteristics of the defect structure are determined by this special arrangement in atoms (Hwang, et al., 2000). In_2O_3 exhibit a cubic bixbyite structure (Marezio, 1966), SnO_2 in contrast has a tetragonal structure (see Fig. 4) similarly to the rutile structure (Enoki, et al., 1991). The density of SnO_2 is 6.95 g/cm^3 (Bates, et al., 1986).

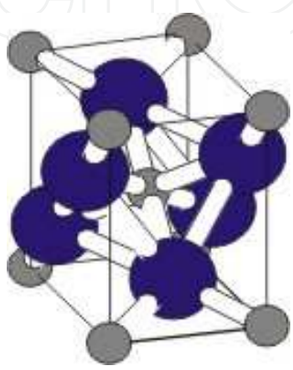

Fig. 5. Tetragonal SnO_2 unit cell.

Indium atoms are incorporated in the lattice as In^{3+} and the tin atoms as Sn^{2+}. The tin atoms have the following electron configuration (Mayr, 1998):

$$Sn : 1s^2 \mid 2s^2\ 2p^6 \mid 3s^2\ 3p^6\ 3d^{10} \mid 4s^2\ 4p^6\ 4d^{10} \mid 5s^2\ 5p^2 \quad (4)$$

It was shown by means of X-ray diffraction analysis (Frank & Köstlin, 1982) that the cubic In_2O_3 structure is preserved by doping with SnO_2 up to the solubility limit of Sn in In_2O_3. The exact solubility limit of Sn in In_2O_3 is not exactly known and varies between 6 ± 2 at.-% of Sn. Up to this concentration every tin atom is substituted by an indium atom. The solubility in thin layers is even higher (Hwang, et al., 2000). The maximum solubility of Indium in the SnO_2 lattice is as low as 1 at.-%. Thereby Sn^{4+} ions are substituted by In^{3+} ions significantly decreasing the electrical conductivity. The ion radius of the Sn^{4+} is 0.71 Å and should lead to a linear reduction of the latticed constant with increasing doping of Sn^{4+} according to the Vegard law (Nadaud, et al., 1998) since the ion radius of In^{3+} is 0.81 Å. However, this is not observed. Udawatte (Udawatte, et al., 2000) reports on a maximum lattice constant reached at 5 mole-% of Sn content dropping below the maximum solubility of 6 mole-% of Sn in the In_2O_3 lattice reported by Nadaud (Nadaud, et al., 1998). These authors have calculated a lattice constant of 10.1247 Å at the maxium solubility limit of Sn compared to a lattice constant of 10.1195 Å that is observed for pure In_2O_3. The presence of Sn strongly changes the behaviour of the oxygen ions. Due to Sn doping the general distance between oxygen and cation increases, but the distance between oxygen and Sn decreases (Nadaud, et al., 1998). Typical phase modifications of indium-tin oxide are listed in the following table.

phase	unit cell	Structure	lattice constant (Å)	density (g/cm^3)
In_2O_3	cubic	Bixbyite	10.117	7.17
SnO_2	tetragonal	Rutile	-	6.95
$In_4Sn_3O_{12}$	rhomboedric	Fluorite	-	7.30

Table 1. ITO phases, unit cells, structures, lattice constants and theoretical desities.

The formation of Indium oxide and the subsequent reaction contributing, inter alia , to the defect structure can be described by Kröger-Vink notation (Rahaman, 1995) according to the following structure elements of the chemical reactions (see Table 2).

abbreviaton		subscript term		superscript term	
V	vacancy	In	In lattic site	x	neutral
In	In atom	O	O lattice site	•	positively charged
O	O atom	i	Interstitial	′	negatively charged
e	electron	g	gas phase		
h	hole				

Table 2. Structure elements of chemical reactions according to Kröger-Vink notation.

The formation of Indium oxide is described according to the following reaction equation:

$$In_2O_3 = 2In^x_{In} + 3O^x_O \leftrightarrow 2In_g + 3/2O_g \quad (5)$$

In parallel to this reaction the formation of gaseous In_2O can occur:

$$2In_g + (1/2O_2)_g \leftrightarrow (In_2O)_g \quad (6)$$

Furthermore In_2O_3 is produced from gaseous In_20_g in oxygen atmospheres according to the following reaction:.

$$In_2O_3 \leftrightarrow 2In^x_{In} + 3O^x_O \leftrightarrow (In_2O)_g + (O_2)_g \quad (7)$$

Taking account of mass action law it is obvious that the oxygen partial pressure controles the number of oxygen vacancies V^x_O. The number of charge carriers in In_2O_3 is thus depending very much on oxygen partial pressure. Theoretically the number of charge carriers would increase at decreasing oxygen partial pressures associated with an increase of electrical conductivity (Mayr, 1998). However, the mechanismen is more complicated in reality since scattering mechanisms can occur consequently decreasing the charge carrier mobility and ion conductivity. More detailed information about scattering mechanisms are given in (Chopra, et al., 1983).

Oxygen vacancy concentration is a function of the defect structure of indium tin oxide (Freeman, et al., 2000). At the beginning first oxygen vacancies start to form as soon as the oxygen atoms leave their interstitial lattice sites ($(2Sn^{\bullet}_{In}O_i'')^x$) and are transformed to gaseous oxygen phase ($1/2O_{2g}$) (Freeman, et al., 2000). The following equation describes the formation of oxygen vacancies and the release of two electrons:

$$(2Sn^{\bullet}_{In}O_i'')^x \leftrightarrow 2Sn^{\bullet}_{In} + (1/2O_2)_g + 2e' \quad (8)$$

Only under reducing conditions ($\sim pO_2^{-1/8}$) oxygen vacancies are formed by diffusing into the bulk from their former lattice sites (O^x_o) (Hwang, et al., 2000). Under extreme reducing conditions ($pO_2 \sim 10^{-14}$ atm) non-reducing defects are formed such as $(2Sn^{\bullet}_{In}3O_OO_i'')^x$ (González, et al., 2001). The equation (9) decribes the transformation of gaseous species whereas two electrons for any oxygen vacancy. Equation (10) shows that the number of oxygen vacancies ($V^{\bullet\bullet}_o$) formed and the number of doped lattice sites ($n = [D^{\bullet}_{In}]$) is a function of oxygen partial pressure ($pO_2^{1/2}$). This relation is described by the equilibrium constant K:

$$O^x_o \leftrightarrow (1/2O_2)_g + V^{\bullet\bullet}_o + 2e' \quad (9)$$

$$K = pO_2^{1/2}[V^{\bullet\bullet}_o]n^2 \quad (10)$$

If one oxygen atom is missing in the unit cell the valance electrons of the surroun-ding atoms have a reduced ionisation energy, which then is provided by thermal lattice vibrations. These electrons are in a quasi-free state and act as conduction electrons. That means that oxygen vacancies provide electrons for the conduction bands (Mayr, 1998). Even in the undoped state small oxygen deficencies can be detected. In this case oxygen vacancies appear in reduced concentrations compared to other defect structures (Hwang, et al., 2000).

system In_2O_3:Sn		
vacancy formation & self-compensation	$2In_{In}^{x} + 2SnO_2 \leftrightarrow (2Sn^{\bullet}_{In}O_i'')^{x} + In_2O_3$	(11)
donator formation	$(2Sn^{\bullet}_{In}O_i'')^{x} \leftrightarrow 2Sn^{\bullet}_{In} + (1/2O_2)_g + 2e'$	(12)
	$O^{x}_{o} \leftrightarrow (1/2O_2)_g + V^{\bullet\bullet}_{o} + 2e'$	(13)
	$2In_{In}^{x} + 2SnO_2 \leftrightarrow 2Sn^{\bullet}_{In} + 2e' + In_2O_3 + (1/2O_2)_g$	(14)

Table 3. Overview of reactions on formation and self-compensation of vacancies as well as formation of donators of the system In_2O_3:Sn according to Kröger-Vink notation.

Nadaud and co-workers investiated oxygen concentration of bulk-ITO by neutron diffraction and Rietveld analysis (Nadaud, et al., 1998). After sintering at 1400 °C in reducing nitrogen atmospheres stoiciometric oxygen concentrations were detected for both undoped and 6 at.-% Sn doped In_2O_3. On the other hand sintering in oxygen atmospheres resulted in bulk oxygen excess of about 3 %. This could be explained by the stoiciometry of the neutral $(2Sn^{\bullet}_{In}O''_i)^{x}$ complexes. Another explanation is the formation of large Sn-based oxygen complexes being difficult to get reduced in the intermediate temperature regime. The same authors investigated these large complexes by Mössbauer, EXAFS and neutron diffraction.

ITO Mössbauer- and EXAFS data von ITO reveal a relaxation of the Sn-O shell similar to the observed relaxation in Sn rhich $In_4Sn_3O_{12}$ (Nadaud, et al., 1998). The analytical data allow to extend the explanation of inefficacy doping above 6 at.-% Sn to the effect that Sn atoms are incorporated at cation sites where they are inactive.

The scientific community is controversial discussing the precipitation of the rhomboedric phase $In_4Sn_3O_{12}$ at Sn concentrations exceeding 6 at.-% Sn. The $In_4Sn_3O_{12}$ structure has been analysed by neutron diffraction experiments and it was ascertaiend that the structure is similar to the Fluorite structure and that a sixfold occupation of M1-sites by Sn cations and sevenfold occupation of M2-sites by In- and Sn cations occurs (Nadaud, et al., 1998). The following figure shows the unit cell of the rhomboedric $In_4Sn_3O_{12}$ phase. The lattice constant is 6.2071 Å and the mismatch angle ø is 99.29°.

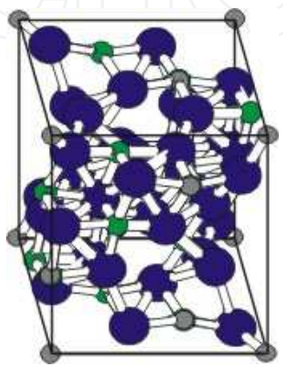

Fig. 6. Unit cell of the $In_4Sn_3O_{12}$ phase.

The atoms of the rhomboedric cells are more densely packed compared to the cubic structure. The rhomoedric phase was fist discovered by Bates et. al. and the density was calculated to 7.303 g/cm^3 (Bates, et al., 1986). It was found by X-ray diffraction experiments that the conformation is a densely packed $M'_mM''_nO_{3m}$ defect structure typically observed for the compositions Yb_7O_2 and Pr_7O_{12}. The In_2O_3 as well as SnO_2 solubility in the $In_4Sn_3O_{12}$-phase is limited (Bates, et al., 1986).

3. Synthesis of nano- and microcrystalline ITO ($Sn:In_2O_3$) and AZO ($Al:ZnO_2$) powders

3.1 ITO powder synthesis

In most cases indium-tin-oxide powders are synthesized by hydrothermal processes. Gel formation is based on the co-precipitation of $InCl_3 \cdot H_2O$ and $SnCl_2$ educts (Udawatte & Yanagisawa, 2000). The microcrystalline powder were homogeneous and reveal the composition of tin doped indium oxide [$In(OH)_3$:Sn] and tin doped indium hydroxide [InOOH:Sn]. Calcination of $In(OH)_3$:Sn at 300 °C resulted in cubic tin doped indium oxide [In_2O_3:Sn]. At calcination temperatures above 500 °C the InOOH:Sn phase is transformed to a solid solution of the formula ($In_2Sn_{1-x}O_{5-y}$). Both powders have been calcinated in air atmosphere. It was found by Mössbauer analysis that the Sn^{4+}-ion coordination number is 8 because each tin atom has 8 neighbouring oxygen atoms which bear opposite charge. A similar synthesis scheme is presented in (Yanagisawa, et al., 2000). In this case indium-tin-oxide has been synthesized from a In-Sn-hydrogel. The hydrothermal treatment of the gel at 300 °C resulted in the formation of InOOH:Sn with mean particle sizes in the range of 80 nm. The subsequent calcination of the product at different calcination temperatures led to different microstructural vacancy configurations of indium tin oxide solid solutions. Calcination at 700 °C lead to a powder with primary particles sizes in the range of about 160 nm. Another approach is the processing of aqueous $In(NO_3)_3 \cdot H_2O$ solutions, subsequent heating and calcination at 500 °C in order to achieve nanosized ITO powders (Sorescu, et al., 2004). The solution of metallic tin and indium in HCl is precipitated by [NH_4OH] (Nam, et al., 2001) and the resulting indium-tin-hydroxide gel is dried, grinded and calcinated at 600 °C.

The processing of tin doped indium oxide crystalites from a direct indium-tin smelting enriched with oxygen is described in (Frank, et al., 1976). The hetero-geneous nucleation process was initiated by small In_2O_3 crystalites. Different compositions and concentration ranges of the smelting process resulted in different tin doping concentrations. Indium tin oxide synthesis by a chemical transport process is reported in (Werner, et al., 1996). Starting from metallic indium and tin and dissolution of the educts in nitric acid the solution is dried and calcinated at 900 °C to achieve In_2O_3 and SnO_2. The mixture of both oxides were doped with transport media iodine, or sulfur, or chlorine. Indium oxide crystals doped with 8.2 mole-% tin and tin oxide crystals doped with 2.4 mole-% indium were attained. These powders have been characterized and the synthesis reactions based on chlorine transport media have been thermodynamically modeled (Patzke, et al., 2000).

In case the seperate oxides are provided as educt materials for the synthesis reaction, indium doped tin oxide, as reported in (Nadaud, et al., 1994) could be processed. In this case In_2O_3 und SnO_2 powder (purity of 99,99 wt.-%) have been mixed in ethanol and calcinated at

1380 °C for theree hours. Colouration from yellow to green and XRD peaks of indium-tin-oxide without exception proved the complete transforma-tion to indium tin oxide.

An alternative ITO synthesis process is given in (Stenger, et al., 1999). Here molten metallic indium tin alloy has been reacted with oxygen in a plasma arc furnace. The product is subsequently quenched by a gas stream at cooling rates between 10^5 K/s to 10^8 K/s to a final temperature between +50 °C and +400 °C. Thereby mixed indium tin oxide powders were produced with specific surface area of 3 m^2/g at maximum. As the powder tends to formation of large agglomerates the size of different ramifications has been analysed by electron microscopy and documented as primary particle size being in the range of 0.03 µm up to 1.0 µm. Hot melt spraying of indium tin melts in oxydizing atmospheres and subsequent quenching is also suitable to process indium tin oxide powders. The agglomerated particle are porous and reveal particle sizes up to 170 µm (see Figure 4).

Compared to this the commercial powder ZY-ITO (Dow Chemical Co. Ltd.) is composed of a mixture of 90 wt.-% In_2O_3 and 10 wt.-% SnO_2, with a specific surface area of 32.0 m^2/g and a mean primary particle size in the range of 3.4 µm.

3.2 AZO powder synthesis

Although various studies of synthesis, characterization and application of Al:ZnO thin layer systems are given in the literature (Stanciu, et al., 2001, Selmi, et al., 2008), there are only a few investigations referring to synthesis and processing of nanosized Al:ZnO particles. Flame spray pyrolysis of liquid Al- ad Zn precursors led to uncontrolled Al:ZnO stoichiometries and segregations of the spinel and wurzite phase combined with evaporation of the metallic Zn phase (Kim, 2008). Vapour condensation (Strachowski, et al., 2007) and spray pyrolysis (Hsiao, et al., 2007) as well as low-pressure spray pyrolysis (Hidayat, et al., 2008) resulted in highly agglomerated particles exhibiting poor redispersing characteristics.

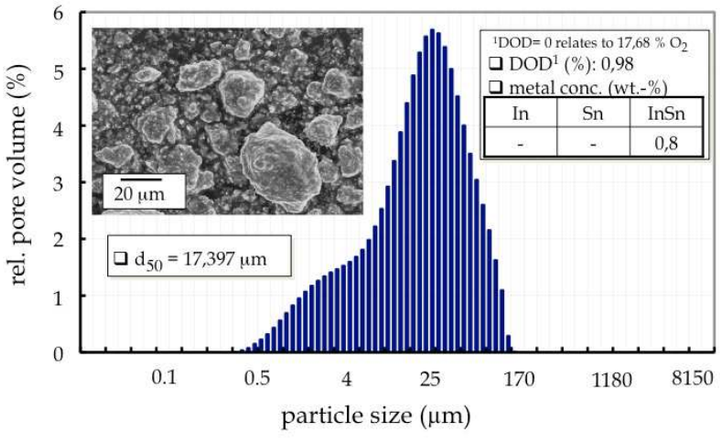

Fig. 7. Indium tin oxide powder produced by hot melt spraying and subsequent quenching: Pore volume of the powder as a function of particle size.

The processing of suitable AZO particles for optoelectronic applications is therefore still challenging. Several alternative processing routes have been elaborated with limited

success. AZO particles synthesized by co-precipitation (Nayak, et al., 2007, Aimable, et al., 2010, Shui, et al., 2009) and solvothermal decomposition (Thu & Maenosono, 2010) are characterized by wide particle size distributions and heterogeneous Al doping concentrations of the microstructure. Hydrothermally (Piticescu, et al., 2006) and sol-gel based processing (Chen, et al., 2008) of AZO particles resulted in particles of high agglomeration degree and mean particles diameters considerably higher than 30 nm and undefined redispersing behaviour. The sintering and densification kinetics of Al:ZnO green bodies is slowed down with increasing Al doping concentrations and the grain growth effects are significantly reduced (Han, et al., 2001, Hynes, et al., 2002). Information about processability of synthesized AZO particles within technical and functional ceramic processing chains is still missing.

4. Sintering of TCO materials

4.1 Sintering and Degree of Oxygen Deficiency (DOD)

The degree of oxygen deficiency (DOD) is referred to oxygen deficient in relation to oxygen concentration of the fully oxidized powder (Schlott, et al., 1995). In (Weigert, et al., 1992) the degree of oxygen deficiency is defined as follows:

$$DOD = (a-b) / (a-c) \tag{15}$$

Here a is the oxygen concentration of stoiciometric oxidic compound, b is the oxygen concentration of the partially reduced oxidic compound and c is the oxygen concentration of the completely reduced metallic compound. The degree of oxygen deficiency is closely related to the oxygen vacancies contributing in parts to the electrical conductivity of ITO. Oxygen release is caused by thermolysis of the ITO powder and oxygen uptake is observed during cooling. The arrangement of oxygen vacancies is likely to be closely connected to the powder synthesis.

Thermal treatment in air leads to light-green colouring of the powder and thermal treatment in reducing atmospheres results in black colouring of the powder. Sputtering is causing a yellow colour of the target (Otsuka-Matsua-Yao, et al., 1997). After sintering the powder can also change colour to dark green or black(Udawatte, et al., 2000). The thermal history of the powder is of significant importance since the powder characteristics are closely correlated with the target quality having a profound impact on the characteristics of the sputtered thin layers (Weigert, et al., 1992).

Evidence proves that oxygen release and uptake of ITO follows a chemical hysteresis (Otsuka-Matsua-Yao, et al., 1997). In repeated heating and cooling cycles different quantities of oxygen are incorporated or released. According to the findings of experimental sintering investigations (Otsuka-Matsua-Yao, et al., 1997) the quantities of released oxygen below 773 K was marginal. A preliminar thermolysis at 1073 K was needed to release carbon monoxide absorbed on the surface. The authors came to the result, that the thermodynamic oxygen characteristics of ITO samples were changed during heating and cooling cycles. Hereby the total oxygen concentration is reduced during each cycle and the kinetics of oxygen release is slowed down cycle by cycle. The initiation temperaure of oxygen release was observed to increase on every iteration of heating and cooling cycle. It was assumed by the authors that there are several phases and several phase transformations inbetween these cycles causing

the discontinuous oxygen release. The related phases exhibit similar chemical composition and resemble the CaF_2 structure. The phases are devided in coherent domaines and the surface energy could have a major impact on the *Gibb's free energy*. This means that chemical hysteresis appears and the oxygen concentration can not be determined explicitly as a function of the temperature and the oxygen partial pressure (Otsuka-Matsua-Yao, et al., 1997).

But there is evidence by experimental investigations that several microphases could act as barriers thereby preventing the oxygen release. These microstructures could originate from extended defects, these are sheared structures or domaines, which diverge from each other in therms of chemical compositions on a very small scale. However the exact analysis and qualitiative and quantitative identification of these structures by X-ray diffraction is not possible since they are charcterized by the structure of the rare earth elements, as for example In_4SnO_8, $In_4Sn_2O_{10}$, In_2O_3 etc. The oxygen release could therefore depend on the interfacial energy between these microphases. In sputtering processes partially reduced indium-tin-oxide target materials are preferred in order to achieve thin film characteristics of minimum specific electric resistance and maximum sputtering efficiencies. Partially reduced targets reveal improved electrical and thermal characteristics as well as optimized densification.

The reduction of the powder or sintered body can be achieved by several methods, i.e. sintering in vacuum or reducing atmospheres (H_2, CO, H_2-Ar oder H_2-N_2). Alternatively the specimen can be hot pressed in graphite moulds or carbon releasing materials or the carbon releasing materials can be doped with the specimen (Weigert, et al., 1992). However under these reducing conditions the caculated oxygenn stoichiometry can not be accurately controlled. Target materials with reproducible and uniform degree of oxygen deficiency are preferred, since they guarantee superior sputtering efficiencies and reduced operation and coating times (Weigert, et al., 1992).

Furthermore the adding of reducing agents and ingredients causes normally the formation of metal particles of different sizes considerably larger than 50 µm (Schlott, et al., 1995). The microstructure appears spotty and targets processed by the powder qualities reveal lower fracture toughness characteristics. From this reason the target specimen shall be reduced below 1000 °C and preferably even below 800 °C. The subsequent densification of the powder and/or the sintered body is realized usually by hot isostatic pressing at temperatures above the melting point of the metal indium-tin-phases (Schlott, et al., 1995).

The hydrophilic characteristics of In_2O_3 should be noted. The water uptake from the surrounding atmosphere leads to the transformation of In_2O_3 to $In(OH)_3$. The water absorption capacity is increasing with increased specific surface area (Lippens, 1996).

Ceramic ITO target materials show low thermal conductivities compared to the metallic target materials and are therefore very susceptible to thermal stresses resulting form non-uniform heating during the sputtering process. It is therefore preferred to increase the thermal conductivity within certain limits in order to guarantee improved thermal shock resistance characteristics (Schlott, et al., 2001).

Based on those optimized target materials the sputtering process is able to be performed at higher specific powder densities without resulting in target desintegration due to formation of thermal gradients.

Improved thermal shock resistance characteristics also allow increased sputtering rates and shortened processing and operation times and consequently reduced production cost. At comparable sputtering rate increased thermal conductivity causes decreased target surface temperature and the decreased temperature gradient ensures a reduction of thermal stresses as well as increased reliability and target life time. This is especially true for target materials working as cathodes under pulsed sputtering operation conditions (Schlott, et al., 2001). In the state-of-the-art the thermal conductivity of ITO target materials is in the range of 7 – 10 W/mK.

In principle a high densification of the target materials is desirable, that means the density should exceed 95 % of the theoretical density in order to guarantee exceptable thermal conductivity characteristics. Usually the thermal conductivity could also be increased by partially reduction (Schlott, et al., 2001).

The theoretical melting point of indium-tin-oxide is 2223 °C. However above the temperature of 1600 °C ITO is evaporated due to a critical vapour pressure regime of the indium and tin metal phases (Vojnovich & Bratton, 1975). At a temperature of 1000 °C the vapour pressure of indium is $6.6 \cdot 10^{-5}$ bar and that of tin is $6.6 \cdot 10^{-7}$ bar (Nichols, 1982).

4.2 Specific TCO sintering techniques

4.2.1 Thermal vacuum degassing

Water absorbed in the green body has to be thermally desorbed in order to avoid crack formation and specimen desintegration after sintering and subsequent cooling. This is especially true for capsuled and hot isostatically pressed samples. The gas formation during sintering has to be prevented by preheating of green bodies within controlled degassing atmospheres as for example N_2 or Ar (Lippens, 1996). The thermal degassing process purifies the grain boundaries and is resulting in a reduction of specific surface area. Hereby the sintering activity is reduced and the densification has to be achieved by pressure assisted sintering techniques (Schlott, et al., 2001).

As referred to the previous section, thermal vacuum degassing exerts a strong influ-ence on the dgree of oxygen deficiency. Other studies (Falk, 2008) came to the result that vauum degassing and combined hot isostatic pressure sintering of capsuled ITO resulted in optimized sintering densities if the vacuum degassing time and temperature is correlated with a defect free micro structure, adopted concentration of free metal species as well as suitable degrees of oxygen deficiency (see Figure 8).

4.2.2 Pre-sintering

Based on the findings of Son (Son & Kim, 1998) it was shown that pressure assisted pre-sintering of In_2O_3 at 5 MPa could increase the densification rate significantly. Dilatometer experiments have proven that maximum densification rates were achieved at 1130 °C and the pressure was increased for another 5 MPa at this temperature. Sintering in air (1 atm) at 1500 °C, however, only leads to a desification of 76 % of the theoretical density.

In (Son & Kim, 1998) it was found, that the agglomerated green structure was transformed in a homogeneous polycrystalline microstructure at temperatures above 1070 °C and the agglomerates showes increased densification rates compared to the surrounding matrix leading to pore formation, so called interagglomerate pores, inbetween the matrix and the

densified microstructure regimes. These pore formations could be effectively prevented by pressure assisted sintering and rearrangement of densified areas and by moving the pores to the surface area.

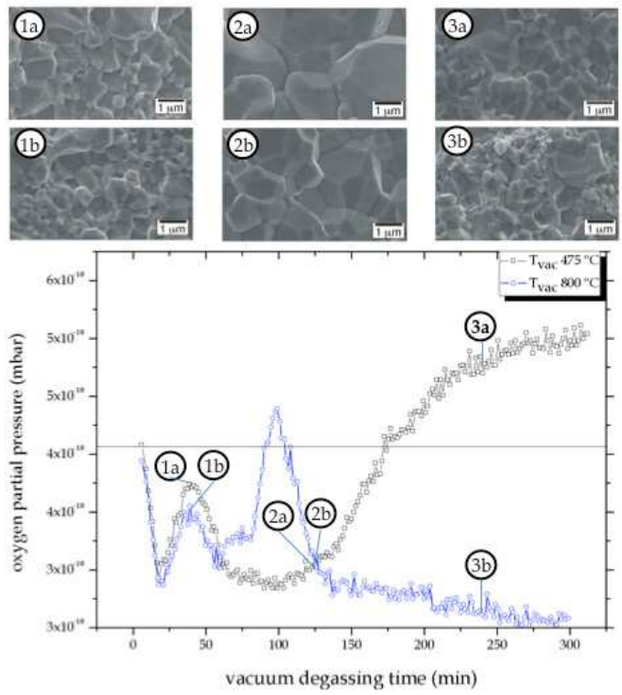

a)

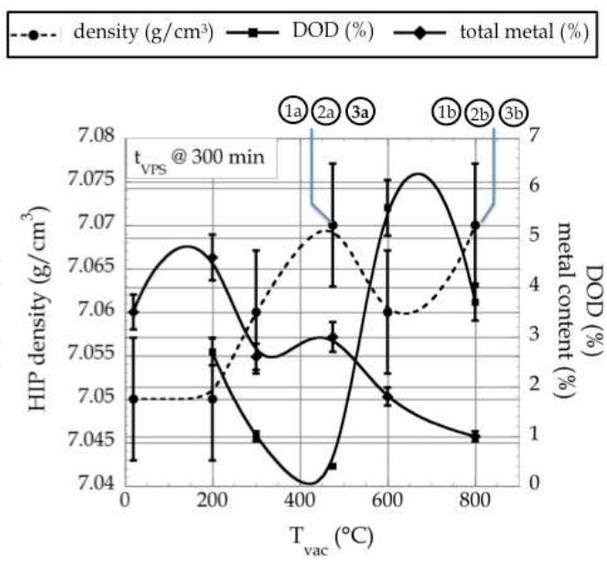

b)

Fig. 8. Oxygen release and oxygen capturing and attained microstructures during vacuum degassing at 475 °C and 800 °C as a function of vacuum degassing time (a), HIP densities, free total metal content and degree of oxygen deficiency (DOD) as a function of vaccum degassing temperature of ITO sintered bodies (b) according to (Andersson, et al. 2005).

4.2.3 Sintering without additives

In (Stenger, et al., 1999) the avoidance of binders and/or dry pressing agents is proposd to prevent any contamination of the received ITO powder. Futhermore it is suggested to avoid the evaporation of gaseous species during pyrolysis of additives since these proceses are likely to reduce efficient pressure build up during hot isostatic pressing.

In (Udawatte, et al., 2000) the group reported about additive-free sintering of ITO powder compacts in air atmospheres. Starting from hydrothermally prepared and at 500 °C calcinated precursors ITO powders of the composition $In_2Sn_{1-x}O_{5-y}$ were attained. The authors have shown previously that pre-sintering of ITO and significant densification is achieved when the $In_2Sn_{1-x}O_5$ phase is transformed to cubic $In_{2-y}Sn_yO_3$ in the temperature range between 1000 °C and 1200 °C. Sintering necks were observed in this temperature range and by excceding the sintering temperature above 1250 °C sigificant grain growth was initiated. At 1300 °C a uniform grain size of 2 µm up to 3 µm and a sintering density of 65% related to the theoretical density was observed.

The maximum densification was achieved at 1450 °C correlated with a mean grain size of about 7 µm. In this case triple grain boundary pores arised more and more frequently compared to intragranular pores.

The conclusion of these experimental investigations were that the sintering is activated mainly in the temperature range between 1300 °C and 1400 °C. The maximum density of about 92 % of the theoretical density was achieved after sintering at 1450 °C for three hours. Furthermore it was concluded that tin doping results in higher densification rates. In (Udawatte, et al., 2000) it is mentioned that tetragonal SnO_2 phase formation counteracts ITO densification.

In (Udawatte & Yanagisawa, 2001) small dry pressed powder compacts (diameter 10 mm, thickness 1.5 mm) have been sintered at 1400 °C for three hours. Taking the theoretical density of 7.106 g/cm^3 as a basis a maximim density of 99.3 % of the theoretical density was achieved. The powder used had a mean particle size of about 80 nm.

Compared to conventional sintering elevated densities have been achieved by „spark plasma sintering“ (SPS) (Takeuchi, et al., 2002). At a reduced dwell time of 5 minutes and high heating rates up to 50 K/min the SPS experiments resulted in considerably low sintering densities, probably due to inhomogeneous temperature distribution.

The sintering of cubic and rhomboedric nanosized ITO powders with mean particle sizes in the range of 50 to 100 nm were sintered up to 900 °C (Kim, et al., 2002) where the cubic phase was transformed. This transformation should theoretically results in a volume expansion of 2.1 % which was not observed since grain growth and pore formation were initiated. It was very complicated to eliminate these pores by subsequent sintering at elevated temperatures. The phase transformation promoted the active diffusion of atoms resulting in inhomogeneous grain growth with intragranular pore formation. It is therefore recommended to prevent phase transformation during sintering in order to achieve higher densification rates and more homogeneous microstructures (Kim, et al., 2002).

4.2.4 Sintering with additives

Vojnovich and co-workers (Vojnovich & Bratton, 1975) investigated the influence of imputities in terms of densification rates of In_2O_3 powders. Combinations of the impurities Si, Ca, Mg, Pb and Fe as well as the doping with Kaolin, Al_2O_3 and SiO_2 have been experimentally studied. It was found that the impurities forming liquid phases due to eutectic reactions even contribute to increased densification rates as for example by doping with Ca, Si and Mg as well as Kaolin. Impurities leading to low melting eutectic phase formations favour liquid phase sintering conditions and resulting in higher density values (Vojnovich & Bratton, 1975). It was found that TiO_2 doping causes an increase of sintering density and limits grain growth. From a concentration of 0.5 wt.-% TiO_2 as sintering additive the phase In_2TiO_5 is precipitated at the grain boundary resulting in increased grain boundary diffusion at reduced diffusion activation energies (Nadaud, et al., 1997).

The influence of Si and Zr impurities on ITO sintering was ivestigated in (Nadaud, et al., 1994). These studies have been motivated by the successful ITO-doping with tetravalent Ti (Nadaud, et al., 1997) and the attempt to achieve even better results with alternative tetravalent doping additives. It came out that a sigificant influence of SiO_2 on ITO densification was not observed. Zirconia, however, has a negative influence on densification and increase specific electrical resistance of ITO ceramics at room temperature. The approach to incorporate sintering additives in order to increase densification is being questioned in (Schlott, et al., 1996), since it was found that imputities, i.e. TiO_2, presented as inclusions or segregations in the microsructure, could cause the formation of nodules.

4.3 Sintering behavior and TCO microstructure

Yanai and Nakamura (Yanai & Nakamura, 2003) found that SnO_2 aggregates in the powder could negatively influence the sintering of ITO and could consequently result in higher porosity of the sintered body. In this case the walls of the pores are covered by SnO_2 segregations. In case of finely distributed SnO_2 segregations decreasing porosity is achieved. And finally in (Hsueh & Jonghe, 1984) it was agreed upon that inhomogeneous sintering takes place in case of heterogeneous density and stress distribution. The experimental evidence of these facts was given by measurements of heterogeneous stress distribution along the grain boundaries causing gradients of the chemical potential and acting as a driving force of the material transport.

Investigations of the microstructure of target materials processed at different processing conditions have shown that finely distributed metallic phases led to improved densification and significant recrystallization of the matrix during hot isostatic pressing.

This means that the liquid metal phase could further enhance the densification although under normal operation condition the wetting of indium oxide and tin oxide by the metallic phases of indium and tin is not observed (Schlott, et al., 1995).

The recrystallization leads to higher densities and and an essantial increase of fracture toughness (Falk, 2007, Falk, 2009) . This is unexpected too, since for ceramic materials a

reduction of grain size leads to improved mechanical properties. Parallel to these findings it was also oberserved that the morphology of partially reduced powders have a major impact on densification and mechanical stability (Schlott, et al., 1995).

Studies of the fracture surface have shown that the intergranular bonding was much higher in recrystallized microstructures. Hereby the metallic phases take over a crack arresting function.

Good quality targets are attained at DOD values in the area of 0.02 to 0.2. If the degree of oxygen deficiency is too low metallic phases are rare and the positive influence of these phases on densification and mechanical strength is neglectable.

If the degree of oxygen deficiency is too high large area metal segregations act as microstructural failures and cause decreasing mechanical strength and worse densification (Schlott, et al., 1995). These authors processed targets of two different powders incoporting metal segregations of mean diameter between 1 μm to 10 μm and < 200 μm. Grain growth effects as a function of the seggregation size was detected and it was conclued that grain growth was especially pronounced in the case of large seggregated microstructures and consequently the maximum sputtering efficiency could not be achieved due to temporarily devating arc discharge at the surface of the target material.

In case of slightly reduced target materials especially tin segregation have been observed and in the event of substantially reduced targets the metallic phases are indentified as InSn alloys. The In-Sn eutectic phase with 48.3 at.-% Sn is melting at 120 °C according to (Shunk, 1969).

4.4 Sintering behavior and electrical conductivity

The electrical conductivity of both pure indium oxide and pure tin oxide is a result of stoichiometry disturbance due to formation of oxygen vacancies. In case of In_2O_3 this structure can be described by the complex $In_2O_{3-x}(V_o)_x e'_{2x}$ (Mayr, 1998). By tin doping, having a higher valence number compared to indium, negative charge carriers are incorporated into the lattice contributing to an additional increase of electrical conductivity.

Freeman and co-workers (Freeman, et al., 2000) have calculated the theoretical distribution of energy bands in tin doped and undoped In_2O_3. In the case of tin doped indium oxide the s-band in the lower section of the conduction band is broadened. Consequently a high mobility of electrons is achieved explaining the high electrical conductivity. Further investigation of electronic ITO structure was elaborated in (Odaka, et al., 2001).

In general the electrical conductivity of Sn doped ITO is lower than theoretically predicted. It was observed that high Sn doping concentrations even reduce the electrical conductivity. The $In_4Sn_3O_{12}$ phase mentioned before is not or slightly electrically conductive (Nadaud, et al., 1998). This fact can be explained by the inactivity of Sn-cations located in M1-positions due to the ternary coordiation of the surrounding oxygen ions. This is similar to the structure of SnO_2 which is neutral. Enventhough In and Sn are located in close vicinity of the periodic system of elements the additional electron of the Sn atom causes a higher affinity to oxygen compared to indium.

The fact that Sn is deteriorating the electrical conductivity becomes more reasonable when high doping levels exceeding 9 at.-% Sn doping concentrations at increased oyxgene partial pressures ($p0_2$ = 1 atm) are applied as it was experimentally proven by Nadaud (Nadaud, et al., 1998).

With the exception of the $In_4Sn_3O_{12}$-phase formation there are mainly two reasons explaining the decrease of electrical conductivity of ITO as soon as doping concentrations exceeding limiting values of 6 at.-% of tin. First the electrical conductivity is reduced due to the formation of the neutral irreducable clusters (Frank & Köstlin, 1982) as for example $(2Sn^{\bullet}_{In}O_i)^x$ complex or the strongly attached and neutral $(Sn_2O_4)^x$ complex (Frank & Köstlin, 1982). Second the lattice is progressively distored as soon as the doping concentration are increased. The atoms are displaced from their original positions and In_2O_3 is similar to SnO_2 crystalline structure. Consequently Sn_2O_i''-cluster are formed acting as neutral lattice defects (Nadaud, et al., 1998). Furthermore these formed clusters are able to restrict doped charge carrier concentrations und decrease charge carrier mobility by causing „*un-ionized impurity scattering*" (Hwang, et al., 2000).

At increasing oxygen vacancy concentrations a compensation process is initiated resulting in a further decrease of the electrical conductivity according to the following equation (Mayr, 1998):

$$O_i'' + V_o \Leftrightarrow O^x_o \tag{16}$$

The electrical characteristics of ITO –phases have been experimentally investigated by Bates and co-workers (Bates, et al., 1986). After sintering of ITO the cubic body centred In_2O_3 phase, being able to incorporate tin concentrations up to 20 mole-% by solid solution process, the rhomboedric $In_4Sn_3O_{12}$ as well as the tetragonal SnO_2 have been detected. It was found that the electrical conductivity is increasing with increased In_2O_3 phase content up to a phase concentration of about 30 mole-%, passing a constant conductivity level up to about 50 mole-% In_2O_3 and reaching a maximum conductivity level at In_2O_3 phase concentration of about 80 mole-%.

This maximum electrical conductivity is a factor of 20 to 25 times higher than the electrical conductivity of pure In_2O_3 (1.6 up to $2.7 \cdot 10^3$ /Ωcm) and a factor of 6 to 20 times higher than the electrical conductivity of $In_4Sn_3O_{12}$ (100 up to 300 /Ωcm). These values are clearly lower than those of thin layers which are in the range of up to 10^4 /Ωcm (Nadaud, et al., 1994).

Studies of the cyclical heating and subsequent cooling of 10 up to 70 mole-% In_2O_3 in air resulted in a reproducible hysteresis of the electrical conductivity and the thermoelectric power. These characteristics are connected to the formation of the high temperature $In_4Sn_3O_{12}$ phase according to the authors (Bates, et al., 1986).

It is also claimed that there are other phase transformations at elevated temperatures, contributing to additional explanations of the fluctuations in electrical conductivity. In continuous thermogravimetrical studies of ITO targets a hysteresis of oxygen uptake and release was observed from multiple cyclical heating and cooling in atmospheres with controlled oxygen partial pressure (Otsuka-Matsua-Yao, et al., 1997). The conclusion is that the microstructural transformation of ITO in the temperature range between 1273 K and

1773 K is correlated with the oxygen content. These results also indicate that the typical ITO characteristics not only depend on a specific oxygen concentration range since a hysteresis is present. Investigations of electrical In_2O_3 characteristics at elevated temperatures have been elaborated by De Wit (Wit, 1975). Hwang (Hwang, et al., 2000) proposed three different regimes of electrical conductivity as a function of oxygen partial pressure and tin concentration. These three regimes have been ascertained experimentally by electrical conductivity and thermoelectric power measurements. The thermoelectric power is a measurement for the thermal diffusion current which is achieved by a temperature gradient. The first regime is characterized by low oxygen partial pressure ($\sim pO_2^{-1/6}$) and low tin doping concentrations. The second regime is distinguished by mean oxygen partial pressure ($\sim pO_2^{0}$) and mean tin concentrations and the third regime by high oxygen partial pressure ($\sim pO_2^{-1/8}$) and high tin doping concentrations. The different doping concentrations result in different defect structures.

The electrical conductivity of bulk nano-ITO is significantly lower compared to the electrical conductivity of bulk µ-ITO. The explanation seems to be that the charge carrier density and the mobility of charge carriers is much lower in nano-ITO (Hwang, et al., 2000). Modeling of optical and electrical characteristics of ITO-thin films made of nano-ITO have been elaborated by Granqvist and co-workers (Ederth, et al., 2003).

5. Conclusions and future trends

Ceramic transparent conductive oxides are widely used for the processing of thin transparent conductive oxides films by vacuum sputtering techniques. These thin film layers are used in liquid crystal display technologies and various application fields such as energy conservation, information storage, electrophotography, electromagnetic radiation shielding and optoelectronic industry. In order to achieve maximum electrical and thermal conductivities and high sputtering efficiencies usually TCO target materials with distinct degrees of oxygen deficiencies are being used. The transparent semiconductor indium-tin-oxide with its high transmission for visible light, its high electrical conductivity and its strong plasma reflection in the near infrared is one of the most common transparent conductive materials. A simplified description of basic understanding of most important ITO characteristics are given and correlated to the desired microstructural properties of sintered TCO target materials.

Specific sintering techniques, i.e. hot isostatic pressing of vacuum pre-sintered, compacted and capsuled ITO bodies results in a distinct consolidation of microstructure and a homogenisation of ITO phase and thus to an increase in HIP sintered density close to the theoretical density. In order to achieve homogeneous microstructures with small mean grain sizes of the pure ITO phase elaborate demands on specific sintering methodologies and adopted sintering processing chains have to be applied. It is important to note that the characteristics of industrially available raw powders in terms of phase composition, particle size distribution, powder density, degree of oxygen deficiency and concentrations of free metal species such as In, Sn and InSn intermetallics could have considerable impact on the quality of the later ITO product. The assessment of superior powder quality in the framework of stream lined and rationalized powder synthesis and processing can therefore be seen as a way forward to realize further optimization of ITO target materials for

sputtering applications. Facing the shortage of indium raw material resources it will be of increasing importance within the coming decades to develop suitable substitute TCO materials. At present aluminium doped zinc oxide (AZO) is one of the most promising candidates. Although the attempts of development of flexible transparent electrode coatings on the base of TCO nano powders for large scale applications have yet to yield any spectacular breakthroughs, new cost-effective niche applications, i.e. flexible displays, are likely to rise up and compete with the state-of-the-art sputtering thin film methodologies in the near future. It is therefore expected that new modern sintering techniques of nano particulate TCO materials, i.e. laser treatment, will be developed in order to significantly improve electrical conductivity of TCO particulate materials on polymer substrates.

6. References

Aimable, A., et al. (2010). Comparison of two innovative precipitation systems for ZnO and Al-doped ZnO nanoparticle synthesis. *Processing and Application of Ceramics,* Vol. 4, No. 3, pp. 107-114, ISSN 1820-6131

Anders, A., et al. (2010). High quality ZnO:Al transparent conducting oxide films synthesized by pulsed filtered cathodic arc deposition. *Thin Solid Films,* Vol. 518, No. pp. 3313-3319, ISSN 0040-6090

Andersson, L., et al. (2005). On a Correlation Between Chemical Hysteresis and Densification Behavior of SnO_2-In_2O_3 Powder Compacts *cfi/Ber. Dtsch. Keram. Ges.*, Vol. 13, No. pp. 208-211, ISSN 0173-9913

Bates, J. L., et al. (1986). Electrical conductivity, Seebeck coefficient, and structure of In_2O_3-SnO_2. *Am. Ceram. Soc. Bull.,* Vol. 65, No. 4, pp. 673-678, ISSN 0002-7812

Carlin, J. F. (2007). Indium, In: *Minerals Yearbook: Metals and Minerals*, J. H. DeYoung, J., pp. 78-79, U.S. Department of the Interiour, U.S. Geological Survey, ISBN 978-1-4113-3015-3, Washington

Chen, K. J., et al. (2008). The crystallization and physical properties of Al-doped ZnO nanoparticles. *Appl. Surf. Sci.,* Vol. 254, No. pp. 5791–5795, ISSN 0169-4332

Chopra, K. L., et al. (1983). Transparent conductors - a status review. *Thin solid films,* Vol. 102, No. pp. 1-46, ISSN 0040-6090

Ederth, J., et al. (2003). Indium tin oxide films made from nanoparticles; models for the optical and electrical properties. *Thin Solid Films,* Vol. 445, No. pp. 199-206, ISSN 0040-6090

Ellmer, K., et al. (2008). *Transparent Conductive Zinc Oxide*, Springer Verlag, ISBN 978-3-540-73611-9, Berlin, Heidelberg, New York

Enoki, H., et al. (1991). The intermediate compound in the In_2O_3-SnO_2 system. *J. Mater. Sci.,* Vol. 26, No. 15, pp. 4110-4115, ISSN 0022-2461

Falk, G. (2008). Densification of $(In_{0,9}Sn_{0,1})_2O_3$ by vacuum pre-sintering and hot isostatic pressing. *cfi/Ber. Dtsch. Keram. Ges.*, Vol. 85, No. 13, pp. 35-38, ISSN 0173-9913

Falk, G. (2009). Heißisostatisches Pressen nanokristalliner Oxidkeramiken, In: *Technische Keramische Werkstoffe*, Kriegesmann, J., pp. 1-37, HvB-Verlag, ISBN 978-3-938595-00-8, Ellerau

Falk, G. (2007). Optimierung von ITO-Targets durch Hippen. *Fortschrittsberichte der DKG: Verfahrenstechnik,* Vol. 21, No. 1, pp. 102-111, ISSN 0173-9913

Frank, G., et al. (1976). The solubilities of Sn in In_2O_3 and of In in SnO_2 crystals grown from Sn-In melts. *J. Cryst. Growth,* Vol. 36, No. 1, pp. 179-180, ISSN 0022-0248

Frank, G. & Köstlin, H. (1982). Electrical properties and defect model of tin-doped indium oxide layers. *Appl. Phys. A,* Vol. 27, No. pp. 197-206, ISSN 1432-0630

Freeman, A. J., et al. (2000). Chemical and thin-film strategies for new transparent conducting oxides. *MRS Bulletin,* Vol. No. August, pp. 45-51, ISSN 0883-7694

Gehman, B. L., et al. (1992). Influence of manufacturing process of indium tin oxide sputtering targets on sputtering behavior. *Thin Solid Films,* Vol. No. 220, pp. 333-336, ISSN 0040-6090

González, G. B., et al. (2001). Neutron diffraction study on the defect structure of indium-tin-oxide. *J. Appl. Phys.,* Vol. 89, No. 5, pp. 2550-2555, ISSN 0021-8979

Granqvist, C. G. & Hultaker, A. (2002). Transparent and conducting ITO films: New developments and applications. *Thin solid films,* Vol. 411, No. 2002, pp. 1-5, ISSN 0040-6090

Han, J., et al. (2001). Densification and grain growth of Al-doped ZnO. *J. Mater. Res.,* Vol. 16, No. 2, pp. 459-468, ISSN 2044-5326

Hidayat, D., et al. (2008). Single crystal ZnO:Al nanoparticles directly synthesized using low-pressure spray pyrolysis. Mat. Sci. Eng. B, Vol. 151, No. pp. 231–237, ISSN 0921-5107

Hsiao, K.-C., et al. (2007). Synthesis, characterization and photocatalytic property of nanostructured Al-doped ZnO powders prepared by spray pyrolysis. *Mat. Sci. Eng. A,* Vol. 447, No. pp. 71-76, ISSN 0921-5093

Hsueh, H. H. & Jonghe, L. C. D. (1984). Particle rotation in early sintering. *J. Am. Ceram. Soc.,* Vol. 67, No. 10, pp. C215-C217, ISSN 0002-7820

Hwang, J. H., et al. (2000). Point defects and electrical properties of Sn-doped In-based transparent conducting oxides. *Solid State Ionics,* Vol. 129, No. pp. 135-144, ISSN 0167-2738

Hyatt, E. P. (1989). Continuous Tape Casting for Small Volumes. *Ceramic Bulletin,* Vol. 68, No. 4, pp. 869-870, ISSN 0002-7812

Hynes, A. P., et al. (2002). Sintering and characterization of nanophase zinc oxide. *J. Am. Ceram. Soc.* , Vol. 85, No. 8, pp. 1979-1987, ISSN 0002-7820

Kim, B. C., et al. (2002). Effect of phase transformation on the densification of coprecipitated nanocrystalline indium tin oxide powders. *J. Am. Ceram. Soc.,* Vol. 85, No. 8, pp. 2083-2088, ISSN 0002-7820

Kim, M. (2008). Mixed-metal oxide nanopowders by liquid-feed flame spray pyrolysis (LF-FSP): Synthesis and processing of core-shell nanoparticles, Ph.D., The University of Michigan, Michigan

Kukla, R., et al. (1998). Sputtered ITO-layers: new approaches for high-quality, low-cost-production, *Proceedings of twelth international conference on vacuum web coating conference*, pp. 104-111, Reno, Nevada

Lippens, P. (1996). Integration of target manufacturing in the sputtering plant, *Proceedings of 39th Annual Technical Conference Proceedings*, pp. 424-430, Albuquerque, ISSN 0737-5921

Marezio, M. (1966). Refinement of the crystal structure of In_2O_3 at two wavelengths. *Acta Cryst.,* Vol. 20, No. pp. 723-728, ISSN 1600-5724

Mayr, M. (1998). High vacuum sputter roll coating: a new large-scale manufacturing technology for transparent conductive ITO layers, Leybold-Heraeus, Report

Nadaud, N., et al. (1995), Matériau pour cible de pulverisation cathodique, EU 0679731, Patent, Saint Gobain Vitrage International

Nadaud, N., et al. (1997). Titania as a sintering additive in indium oxide ceramics. *J. Am. Ceram. Soc.,* Vol. 80, No. 5, pp. 1208-1212, ISSN ISSN 0002-7820

Nadaud, N., et al. (1998). Structural studies of tin-doped indium oxide (ITO) and $In_4Sn_3O_{12}$. *J. Solid State Chem.,* Vol. 135, No. 1, pp. 140-148, ISSN 1095-726X

Nadaud, N., et al. (1994). Sintering and electrical properties of titania- and zirconia-containing In_2O_3-SnO_2 (ITO) ceramics. *J. Am. Ceram. Soc.,* Vol. 77, No. 3, pp. 843-46, ISSN 0002-7820

Nam, J. G., et al. (2001). Synthesis and sintering properties of nanosized In_2O_3-10 wt.-% SnO_2 powders. *Scripta Mater.,* Vol. 44, No. 8-9, pp. 2047-2050, ISSN 1359-6462

Nayak, J., et al. (2007). Yellowish-white photoluminescence from ZnO nanoparticles doped with Al and Li. *Superlattices and Microstructures,* Vol. 42, No. pp. 438–443, ISSN 0749-6036

Nichols, D. R. (1982). ITO films: adaptable to many applications. *Photonics Spectra,* Vol. No. pp. 57-60, ISSN 0731-1230

Odaka, H., et al. (2001). Electronic structure analyses of Sn-doped In_2O_3. *Jpn. J. Appl. Phys.,* Vol. 40, No. 5A, pp. 3231-3235, ISSN 0021-4922

Otsuka-Matsua-Yao, S., et al. (1997). Chemical hysteresis on the release and uptake of oxygen by SnO_2-doped In_2O_3 powders. *J. Electrochem. Soc.,* Vol. 144, No. 4, pp. 1488-1494, ISSN 0013-4651

Patzke, G. R., et al. (2000). Chemischer Transport fester Loesungen. 8. Chemischer Transport und Sauerstoffionenleitfaehigkeit von Mischkristallen im System In_2O_3/SnO_2. *Z. Anorg. Allg. Chem.,* Vol. 626, No. 11, pp. 2340-2346, ISSN 1521-3749

Piticescu, R. R., et al. (2006). Synthesis of Al-doped ZnO nanomaterials with controlled luminescence. *J. Eur. Ceram. Soc.,* Vol. 26, No. pp. 2979–2983, ISSN 0955-2219

Rahaman, M. N. (1995). *Ceramic processing and sintering*, Marcel Dekker, Inc., ISBN 0-8247-9573-3, New York

Schlott, M., et al. (2001), Method of preparing indium oxide/tin oxide target for cathodic sputtering, US 6187253, Leybold Materials GmbH, Patent

Schlott, M., et al. (1996). Nodule formation on indium-oxide tin-oxide sputtering targets, *Proceedings of 1996 SID International Symposium*, Santa Anna, CA, USA

Schlott, M., et al. (1995), Target für die Kathodenzerstäubung zur Herstellung transparenter, leitfähiger Schichten und Verfahren zu seiner Herstellung, DE 4407774, Patent, Leybold Materials GmbH

Selmi, M., et al. (2008). Studies on the properties of sputter-deposited Al-doped ZnO films. *Superlattices and Microstructures,* Vol. 44, No. pp. 268–275, ISSN 0749-6036

Shui, A., et al. (2009). Preparation and properties for aluminum-doped zinc oxide powders with the coprecipitation method. *J. Ceram. Soc. Japan,* Vol. 117, No. 5, pp. 703-705, ISSN 1882-1022

Shunk, F. A. (1969). *Constitution of binary alloys* (2 supplement), McGraw-Hill, Inc., ISBN 07-057315-8, Chicago

Son, J. W. & Kim, D. Y. (1998). Enhanced densification of In_2O_3 ceramics by presintering with low pressure (5 MPa). *J. Am. Ceram. Soc.,* Vol. 81, No. 9, pp. 2489-2492, ISSN 0002-7820

Sorescu, M., et al. (2004). Nanocrystalline rhombohedral In_2O_3 synthesized by hydrothermal and postannealing pathways. *J. Mater. Sci.,* Vol. 39, No. pp. 675-677, ISSN 1573-4838

Stanciu, L. A., et al. (2001). Effects of Heating Rate on Densification and Grain Growth during Field-Assisted Sintering of α-Al_2O_3 and $MoSi_2$ Powders. *Metall. Mater. Trans. A,* Vol. 32, No. pp. 2633-2638, ISSN 1073-5623

Stenger, B., et al. (1999), Verfahren zum Herstellen eines indium-Zinn-Oxid-Formkörpers, DE 19822570, Patent, W.C. Heraeus GmbH

Strachowski, T., et al. (2007). Morphology and luminescence properties of zinc oxide nanopowders doped with aluminum ions obtained by hydrothermal and vapor condensation methods. *J. Appl. Phys.,* Vol. 102, No. 7, pp. 073513 - 073513-9 ISSN 0021-8979

Straue, N., et al. (2009). Preparation and soft lithographic printing of nano-sized ITO-dispersions for the manufacture of electrodes for TFTs. *J. Mater. Sci.,* Vol. 44, No. 22, pp. 6011-6019, ISSN 1573-4838

Takeuchi, T., et al. (2002). Rapid preparation of indium tin oxide sputtering targets by spark plasma sintering. *J. Mater. Sci. Lett.,* Vol. 21, No. pp. 855-857, ISSN 0261-8028

Thu, T. V. & Maenosono, S. (2010). Synthesis of high-quality Al-doped ZnO nanoink *J. Appl. Phys.* , Vol. 107, No. 1, pp. 014308-014308-6, ISSN 0021-8979

Udawatte, C. P. & Yanagisawa, K. (2001). Fabrication of low-porosity indium tin oxide ceramics in air from hydrothermally prepared powders. *J. Am. Ceram. Soc.,* Vol. 84, No. 1, pp. 251-53, ISSN 0002-7820

Udawatte, C. P. & Yanagisawa, K. (2000). Hydrothermal preparation of highly sinterable tin doped indium oxie powders: the effect of the processing parameters, *Proceedings of Ceramic Processing Science VI*, Inuyama City, Japan,

Udawatte, C. P., et al. (2000). Sintering of additive free hydrothermally derived indium tin oxide powders in air. *J. Solid State Chem.,* Vol. 154, No. 2, pp. 444-450, ISSN 0022-4596

Vojnovich, T. & Bratton, R. J. (1975). Impurity effects on sintering and electrical resistivity of indium oxide. *Am. Ceram. Soc. Bull.,* Vol. 54, No. 2, pp. 216-217, ISSN 0002-7812

Warschkow, O., et al. (2003). Defect structures of tin-doped indium oxide. *J. Am. Ceram. Soc.,* Vol. 86, No. 10, pp. 1700-1706, ISSN 0002-7820

Weigert, M., et al. (1992), Target für die Kathodenzerstäubung und Verfahren zu dessen Herstellung, DE 4124471, Patent, Degussa AG

Werner, J., et al. (1996). Chemical transport of restricted solid solutions of In_2O_3 and SnO_2: experiments and thermodynamic process analysis. *J. Cryst. Growth,* Vol. 165, No. 3, pp. 258-267, ISSN 0022-0248

Wit, J. H. W. d. (1975). The high temperature behaviour of In_2O_3. *J. Solid State Chem.,* Vol. 13, No. pp. 192-200, ISSN 0022-4596

Yanagisawa, K., et al. (2000). Preparation and characterization of fine indium tin oxide powders by a hydrothermal treatment and postannealing method. *J. Mater. Res.*, Vol. 15, No. 6, pp. 1404-1408, ISSN 0884-2914

Yanai, Y. & Nakamura, A. (2003), Manufacturing method of ITO powder with tin dissolved in indium oxide, and manufacturing method of ITO target, US 2003/0039607, Patent,

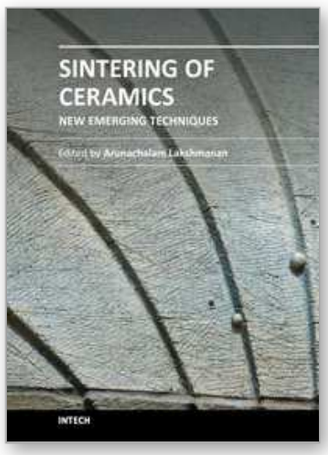

Sintering of Ceramics - New Emerging Techniques

Edited by Dr. Arunachalam Lakshmanan

ISBN 978-953-51-0017-1
Hard cover, 610 pages
Publisher InTech
Published online 02, March, 2012
Published in print edition March, 2012

The chapters covered in this book include emerging new techniques on sintering. Major experts in this field contributed to this book and presented their research. Topics covered in this publication include Spark plasma sintering, Magnetic Pulsed compaction, Low Temperature Co-fired Ceramic technology for the preparation of 3-dimesinal circuits, Microwave sintering of thermistor ceramics, Synthesis of Bio-compatible ceramics, Sintering of Rare Earth Doped Bismuth Titanate Ceramics prepared by Soft Combustion, nanostructured ceramics, alternative solid-state reaction routes yielding densified bulk ceramics and nanopowders, Sintering of intermetallic superconductors such as MgB2, impurity doping in luminescence phosphors synthesized using soft techniques, etc. Other advanced sintering techniques such as radiation thermal sintering for the manufacture of thin film solid oxide fuel cells are also described.

InTech Europe
University Campus STeP Ri
Slavka Krautzeka 83/A
51000 Rijeka, Croatia
Phone: +385 (51) 770 447
Fax: +385 (51) 686 166
www.intechopen.com

InTech China
Unit 405, Office Block, Hotel Equatorial Shanghai
No.65, Yan An Road (West), Shanghai, 200040, China
中国上海市延安西路65号上海国际贵都大饭店办公楼405单元
Phone: +86-21-62489820
Fax: +86-21-62489821

IntechOpen